Intermetallics 55 (2014) 154–161

Contents lists available at ScienceDirect

Intermetallics

journal homepage: www.elsevier.com/locate/intermet

Phase equilibria and mechanical properties of the Ir–W–Al system

T. Omori*, K. Makino, K. Shinagawa, I. Ohnuma, R. Kainuma, K. Ishida

Department of Materials Science, Graduate School of Engineering, Tohoku University, Sendai 980-8579, Japan

ARTICLE INFO

Article history:
Received 10 June 2014
Received in revised form
28 July 2014
Accepted 28 July 2014
Available online 17 August 2014

Keywords:
A. Intermetallics
B. Mechanical properties
B. Phase stability
B. Yield stress
D. Microstructure

ABSTRACT

Phase equilibria in the Ir–W, Ir–Al and Ir–W–Al systems at temperatures between 1100 °C and 1600 °C were experimentally investigated using diffusion couples and two- or three-phase alloys, and the mechanical properties of γ' ($L1_2$) strengthened Ir–W–Al alloys were examined by hardness and compression tests at room and elevated temperatures. The phase boundaries between the γ(A1)/ε'($D0_{19}$), ε'/ε(A3) and $\varepsilon/\varepsilon''$(B19) in the Ir–W system at 1400 °C–1600 °C and those between the γ/β(B2) and $\beta/Al_{2.7}Ir$ in the Ir–Al system at 1100 °C–1400 °C were determined. The phase diagrams in the Ir-rich corner of the Ir–W–Al ternary system at 1300 °C and 1400 °C were also determined. The existence of the γ' phase of the Ir_3(W,Al) ternary compound was confirmed, and this system was found to consist of the γ, γ', ε, ε' and β phases in the Ir-rich portion. It was also found from hardness and compression tests up to 1200 °C that Ir–Al–W alloys having the $\gamma + \gamma'$ structure with a small lattice misfit show high hardness and strength at room and high temperatures.

1. Introduction

Iridium has a high melting temperature of 2447 °C and good corrosion resistance, and iridium and iridium-based alloys are used for high-temperature applications, including crucibles and spark plugs in automobiles despite the limited resource availability. Iridium alloys are often strengthened by solid-solution strengthening [1], and, for example, W is added to Ir alloy containing a small amount of Th and Al developed for fuel cladding in radioisotope thermoelectric generators for space power applications [2]. The Ir solid solution γ phase (A1) can be strengthened by precipitation of the γ' phase with the $L1_2$ phase using Ir_3Nb, Ir_3Ta, Ir_3Zr, Ir_3Hf or Ir_3V as reported by Yamabe–Mitarai et al. [3–16]. This alloy design is similar to that of the Ni-based superalloys with the coherent precipitate of the Ni_3Al γ' phase. The improvement of temperature capability is difficult in Ni-based alloys because the operating temperature is close to the melting temperature of the Ni-based alloys, and Ir-based alloys are expected to be used at higher temperatures beyond those of the Ni-base alloys due to their high melting temperature. However, the oxidation resistance of Ir is poor because of the formation of volatile IrO_3 above 1120 °C [17–19]. It has been reported that the oxidation resistance can be drastically improved in Ir–Al due to formation of an Al_2O_3 layer [17,20,21].

Although there are many kinds of $L1_2$ compounds in the Ir-based binary systems as described above, no γ' phase with the $L1_2$ structure exists in the Ir–Al binary system [22]. Recently, we have found that the γ' phase is stabilized in the Co–Al–W ternary system [23] although metastable Co_3Al and Co_3W with the $L1_2$ structure are observed under very limited conditions [24–28]. Co–Al–W-based alloys strengthened by the γ' phase show promise for use as high-temperature materials because of their stable coherent microstructure and good high-temperature strength [23,29–36]. In analogy with the Co belonging to the same group as Ir in the periodic table, an Ir_3(W, Al) phase with the $L1_2$ structure has been discovered [23], and its stability has also been thermodynamically investigated [37]. The Ir–W–Al ternary alloy shows a coherent $\gamma + \gamma'$ two-phase structure [23], and therefore, this alloy system is important as high-temperature materials. In this study, the phase equilibria in the Ir-rich corner of the Ir–W–Al system at 1400 °C and 1300 °C as well as the Ir–W and Ir–Al binary systems were investigated, and in addition, the mechanical properties were studied.

While no phase diagram of the Ir–W–Al ternary system has been reported, Fig. 1(a) and (b) show phase diagrams of the Ir–W and Ir–Al binary systems, respectively. The diagram of the Ir–W binary system was assessed by Nagender Naidu et al. [38] based on experimental data [39–42]. This phase diagram consists of the liquid, γ (Ir, A1), ε (A3), ε' (Ir_3W, $D0_{19}$), ε'' (IrW, B19), σ (D8b) and α

* Corresponding author. Tel./fax: +81 22 795 7323.
E-mail address: omori@material.tohoku.ac.jp (T. Omori).

http://dx.doi.org/10.1016/j.intermet.2014.07.021
0966-9795/

(W, A2) phases. Although two types of ordered phase ε' and ε'' have been reported [43,44], it has been pointed out that the experimental data on phase equilibria involved with these phases are particularly inadequate [38]. On the other hand, the phase equilibria in the Ir–Al system have been reported by Axler [45], and more recently, they have been examined by many researchers [46–51]. The assessed phase diagram of the Ir–Al system [22] is based on the report by Abe et al. [52], which consists of the liquid, γ (Ir, A1), β (IrAl, B2), solid solution (Al, A1) and other intermetallic compounds, namely, $Al_{2.7}Ir$, Al_3Ir, $Al_{28}Ir_9$, $Al_{45}Ir_{13}$ and Al_9Ir_2. The crystallographic data of the phases in the Ir–W and Ir–Al systems are summarized in Table 1.

2. Experimental

Ir–W binary alloys (Ir–10W, Ir–40W, Ir–60W), Ir–Al binary alloys (Ir–30Al, Ir–65Al) and Ir–W–Al ternary alloys (Ir–4W–8Al, Ir–5W–25Al, Ir–7W–30Al, Ir–10W–9Al, Ir–10W–10Al, Ir-10.5W-12.5Al, Ir–11W–7Al, Ir–11W–9Al, Ir–13W–5Al, Ir–13W–7Al, Ir–16W–5Al, Ir–18W–2Al, Ir–20W–10Al, Ir–20W–20Al) listed in Table 2 (at%) were prepared from Ir (99.9 mass%), W (99.9 mass%) and Al (99.9 mass%) by arc melting under an Ar atmosphere (99.999 vol.%). Since the diffusivity is low in Ir–W alloys due to their high melting temperature and it is difficult to obtain coarse microstructure in two-phase alloys, the diffusion couple (DC) method was employed to determine the phase diagram. In order to obtain DCs, one arc-melted Ir–W alloy ingot was put on the top of the other Ir–W alloy ingot, weight of which is several 10 g, and the upper ingot was partially melted from the top, the current and melting time being adjusted to obtain diffusion zone at interface. The DCs were then annealed at temperatures between 1400 °C and 1600 °C for 168 h in an Ar atmosphere, followed by water quenching. The composition–penetration curves at the corner sections of the DCs were obtained by electron probe microanalysis (EPMA), ZAF correction being applied using the pure elements as standard.

Ir–Al binary alloys with a two-phase structure and Ir–W–Al ternary alloys with a two-phase or three-phase structure were annealed at 1100–1400 °C for 96–672 h and at 1300 °C for 1008 h or 1344 h or at 1400 °C for 1008 h, respectively, where the specimens were wrapped with tungsten sheet or tungsten wire in order to prevent them from reacting with the quartz capsule during heat treatment, which was followed by water quenching. The Ir–30Al alloy and all the Ir–W–Al alloys were homogenized at 1900 °C for 1 h in an alumina crucible before the aforementioned annealing. The composition in each phase was measured by EPMA with the ZAF correction. Phase identification and determination of a lattice

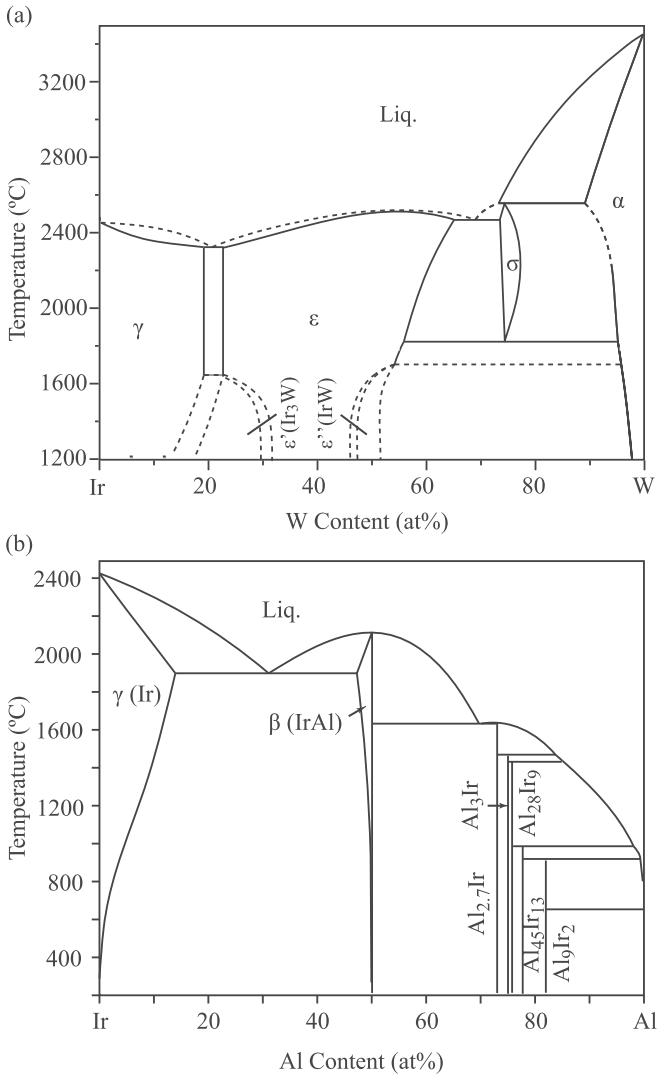

Fig. 1. Phase diagrams of the (a) Ir–W [38] and (b) Ir–Al binary systems [22].

Table 1
Crystal structures of the phases in the Ir–W and Ir–Al systems.

Phase	Composition (at%)	Pearson symbol	Space group	Strukturbericht designation	Prototype
Ir–W binary					
(Ir)	0–19	*cF4*	$Fm\bar{3}m$	*A1*	Cu
ε	22–66	*hP2*	$P6_3/mmc$	*A3*	Mg
ε'	?–30	*hP8*	$P6_3/mmc$	$D0_{19}$	Ni_3Sn
ε''	48–55.5	*oP4*	*Pmma*	*B19*	AuCd
σ	74–78	*tP30*	$P4_2/mnm$	$D8_b$	σCrFe
(W)	90–100	*cI2*	$Im\bar{3}m$	*A2*	W
Ir–Al binary					
(Ir)	0–14	*cF4*	$Fm\bar{3}m$	*A1*	Cu
AlIr	47.5–52.5	*cP2*	$Pm\bar{3}m$	*B2*	CsCl
$Al_{2.7}Ir$	72.5–73.3	*cP32*	*P23*	–	–
Al_3Ir	75	*hP8*	$P6_3/mmc$	$D0_{18}$	Na_3As
$Al_{28}Ir_9$	75.7	*tP**	*P31c*	–	–
$Al_{45}Ir_1$	77.6	*oP232*	*Pnma*	–	–
Al_9Ir_2	81.8	*mP22*	$P2_1/c$	$D8_d$	Co_2Al_9
(Al)	100	*cF4*	$Fm\bar{3}m$	*A1*	Cu

Table 2
Nominal compositions of tested alloys.

Sample composition (at%)	Experiments
Ir–10W	Phase equilibria (diffusion couple)
Ir–40W	Phase equilibria (diffusion couple)
Ir–60W	Phase equilibria (diffusion couple)
Ir–30Al	Phase equilibria
Ir–65Al	Phase equilibria
Ir–4W–8Al	Hardness@RT, HT
Ir–5W–25Al	Phase equilibria
Ir–7W–30Al	Phase equilibria
Ir–10W–9Al	Hardness@RT, compression test
Ir–10W–10Al	Hardness@RT, HT
Ir-10.5W-12.5Al	Hardness@RT, HT
Ir–11W–7Al	Phase equilibria, hardness@RT
Ir–11W–9Al	Hardness@RT
Ir–13W–5Al	Hardness@RT
Ir–13W–7Al	Phase equilibria, hardness@RT
Ir–16W–5Al	Hardness@RT
Ir–18W–2Al	Phase equilibria
Ir–20W–10Al	Phase equilibria
Ir–20W–20Al	Phase equilibria